



Liu, Z., Li, P. and Srikanth, N. (2019) Effect of delamination on the flexural response of [+45/-45/0]_{2s} carbon fibre reinforced polymer laminates. *Composite Structures*, 209, pp. 93-102.

There may be differences between this version and the published version. You are advised to consult the publisher's version if you wish to cite from it.

<http://eprints.gla.ac.uk/172397/>

Deposited on: 1 November 2018

Enlighten – Research publications by members of the University of Glasgow
<http://eprints.gla.ac.uk>

**Effect of delamination on the flexural response of $[+45/-45/0]_{2s}$
carbon fibre reinforced polymer laminates**

Zhe Liu ¹, Peifeng Li ^{2,*}, Narasimalu Srikanth ³

¹ School of Mechanical and Aerospace Engineering, Nanyang Technological University,
Singapore

² School of Engineering, University of Glasgow, Glasgow, UK

³ Energy Research Institute @NTU, Nanyang Technological University, Singapore

* Corresponding author's email: peifeng.li@glasgow.ac.uk (P. Li); Tel: +44 141 330 2703.

Abstract

The damage arising in the manufacturing or service operation can result in the degradation in mechanical properties or even structural failure in composite laminates. This work investigated the flexural behaviour of $[+45/-45/0]_{2s}$ carbon fibre reinforced polymer laminates with the artificially embedded delamination (pre-delamination) at different interfaces. After static flexural experiments, the internal 3D damage including various failure modes was characterised and quantified in the X-ray microtomography. It was found that regardless of the pre-delamination, similar in-ply (fibre failure, matrix cracking and fibre/matrix debonding) and interlaminar (delamination) failure modes occur dominantly in the outer ply group of the compression zone in all the laminates. However, the pre-delamination and its location have the influence on both the distribution and size of the 3D damage, and thus on the flexural properties. The flexural strength that is reduced by pre-delamination is the most (least) sensitive to the pre-delamination embedded at the third (ninth) interface.

Keywords: Laminates; Mechanical properties; Delamination; X-ray tomography.

1 Introduction

Wind turbine blade structures are commonly made of fibre reinforced polymer (FRP) composite laminates that possess good strength-to-weight ratio, corrosion resistance and excellent fatigue properties [1, 2]. Due to the decreasing cost and better properties, carbon fibres have the potential to replace glass fibres in some blade laminates. The manufacturing process may often introduce defects, and the operation or maintenance can further result in the damage in FRP laminates. Porosity, delamination, fibre failure, matrix cracks and fibre/matrix debonding are the common damage types in the laminate. The damage can lead to the degradation in stiffness, strength and fatigue life or even structural failure [3, 4]. Wind turbines are designed to sustain the service for around 20–30 years and thus expected to continue operating even if there is slight damage in the blade. Wind turbine blades in service are subjected to flexural loading caused by aerodynamic and gravitational forces [5-7]. Thus it is necessary to investigate how the existing damage affects the flexural behaviour of FRP laminates.

Delamination is one of the common manufacturing defects and failure modes of FRP laminated composites [8-10]. Many studies have focused on the effect of delamination on mechanical properties of FRP laminates [3, 11-15]. Wang et al. [13] conducted compression experiments and finite element analysis to reveal the compressive failure mechanism in glass fibre reinforced polymer (GFRP) laminates containing embedded pre-delamination. Finite element modelling has also been applied to probe the uniaxial buckling behaviour of unidirectional and cross-ply carbon fibre reinforced polymer (CFRP) laminates with the delamination damage [11]. Aslan and Sahin [3] reported that the large delamination induced by low velocity impact can influence the buckling behaviour and compressive failure in GFRP

laminates. However, there is a paucity of research on the flexural behaviour of FRP laminated composites that contain the existing delamination.

There are different non-destructive techniques to characterise the damage within FRP laminates and to determine how the damage degrades mechanical properties. X-ray microtomography (μ XT, also commonly abbreviated as μ CT in the literature) has been the powerful tool to reveal the internal 3D microstructures of materials with the resolution down to microns [16-19]. In particular, the μ XT technique has been used to investigate the damage in FRP laminates [19-26]. Schilling et al. [26] extracted the internal micro-cracks in graphite/epoxy laminates after fatigue failure using the μ XT. Moffat et al. [25] observed the damage evolution in the $[90/0]_s$ CFRP laminate under tension in the in-situ synchrotron μ XT. Lambert et al. [23] tracked the damage patterns within the $[+45/-45/0]_{3s}$ GFRP laminates during the fatigue tests. However, only few studies have reported the quantitative analysis of μ XT images to measure the damage in FRP laminates and relate it to degraded mechanical properties [21, 24].

The aim of this study was to investigate the effect of embedded pre-delamination (i.e., pre-existing delamination) on the flexural behaviour of CFRP laminates with the symmetric layup sequence $[+45/-45/0]_{2s}$. The artificial pre-delamination was embedded at one of the different interfaces in the laminates. Static three-point bending flexural tests were performed to measure the flexural properties of the laminates with or without the pre-delamination. The μ XT was conducted to characterise the internal damage of the laminates after the flexural failure under the first loading. The area of the damage in different orientations was quantified and correlated to the reduction of flexural properties by reloading. After the reloading failure, the fracture surfaces of the laminates were examined in the scanning electron microscope (SEM) to reveal the mechanisms for different failure modes. In addition,

the stress in the laminate with no pre-delamination was analysed using the classical laminate theory (CLT) and then used to predict the failure in the laminate.

2 Experimental procedure

2.1 Materials and specimens

The carbon fibre reinforced polymer laminates were fabricated with the L-930HT (Cytec Solvay Group, USA) flame retardant unidirectional epoxy carbon prepregs. The L-930HT prepreg is extremely flame retardant that allows the designer to use it in a wide variety of structural applications, e.g., potentially wind turbine blades. The layup sequence is symmetric $[+45/-45/0]_{2s}$, which is extensively used in wind turbine blade laminate structures. Seven types of laminates were prepared with or without the pre-delamination. One of them was with no pre-delamination (NPD). A 20 μm thick and 12 mm wide Teflon layer was embedded at the first (+45/-45), second (-45/0), third (0/+45), ninth (+45/0), tenth (0/-45) and eleventh (-45/+45) interface to create the pre-delamination in the other six types of laminates that were named PD1, PD2, PD3, PD9, PD10 and PD11, respectively (Fig. 1). The pre-delamination location in the PD1, PD2 and PD3 laminates was symmetric about the neutral plane in relation to the PD11, PD10 and PD9 laminates, respectively. Table 1 lists the ply configuration in the seven types of CFRP laminates; PD represents the embedded pre-delamination.

The 190 \times 250 mm rectangular laminates were cured in the autoclave at 127°C for 60 min under the vacuum pressure of -0.069 MPa (i.e., 0.069 MPa lower than the atmospheric pressure). The pressure inside the chamber was maintained at 0.41 MPa during the whole curing process. After curing, the thickness (i.e., depth) of all the laminates was measured to be approximately 2.13 mm and the weight fraction of

fibres was nearly 70%. The specimens of the length 150 mm and the width 12 mm were machined from the cured laminates by waterjet cutting for static flexural testing (Fig. 1). For the specimens with the pre-delamination, the 12 × 12 mm square Teflon layers was in the central portion of the specimen.

2.2 *Static flexural testing and X-ray microtomography*

Static flexural tests were conducted on the 150 × 12 mm laminate specimens in an in-house three-point bending fixture in the MTS 810 (MTS Systems Corp., USA) servohydraulic universal testing machine according to ASTM D790. The three-point bending fixture fabricated with high stiffness steel was clamped with the wedge grips by the high pressure hydraulics. The crosshead velocity was 2 mm min⁻¹ and the support span length was 75 mm. Eight specimens were tested for each type of laminates. Flexural properties of various composite laminates have been investigated under three-point bending loads in the literature [27-29]. Note that even though three-point bending testing is principally designed for materials that fail at relatively small deflections and for the determination of flexural modulus, ASTM D790 standard provides the correction method to calculate the flexural stress at large deflections of more than 10% of the support span. The failure is identified at the point when the flexural stress reaches the maximum and then drops abruptly.

After the failure, three out of the eight tested specimens were scanned in the X-ray microtomography at 55 kV and 46 μA to characterise the internal damage near the central portion of the specimen. A set of 720 projections was recorded as the specimen rotated 360°, from which the 3D image of the specimen was reconstructed by an in-house algorithm [18, 30]. The algorithm stretched the depth of the image volume. The spatial resolution of the μXT images was 7.0 μm in the longitudinal

(length) and transverse (width) direction and 8.8 μm in the depth direction, respectively. The damage (e.g., delamination, transverse cracks and fibre failure) was visualised and quantified for each ply and interface in the specimen using the AVIZO/FIRE software.

After the μXT characterisation, all the specimens were subjected to static flexural reloading to determine the residual modulus and strength. After the reloading failure, the fracture surfaces at the interfaces inside the specimens were examined in the JEOL (JEOL Ltd, Japan) 5600LV SEM.

3 Stress analysis

Analysis based on the classical laminate theory was performed to predict the in-plane stresses of the $[+45/-45/0]_{2s}$ laminate with no pre-delamination subjected to the three-point bending load. The interlaminar shear stresses were determined according to the principle of continuum mechanism [27, 31]. Table 2 lists the anisotropic mechanical properties of unidirectional (UD) laminae required for the stress analysis. These mechanical properties except ν_{23} , G_{23} and S_{23} were directly measured in the compression (ASTM D3410), tension (ASTM D3039) and shear (ASTM D7078) experiments on the UD laminae. The Poisson's ratio $\nu_{23} = 0.3$ was obtained in the literature [32], thus the transverse shear modulus $G_{23} = E_2 / (1+\nu_{23})$ [33]. The transverse shear strength S_{23} was approximated by the measured in-plane shear strength ($S_{12} = S_{13}$). In the CLT analysis of three-point bending, the $[+45/-45/0]_{2s}$ laminate was subjected to a bending moment M_y ,

$$M_y = \frac{P_f L}{4} \quad (1)$$

where $P_f = 343 \text{ N}$ is the average failure load as measured in the flexural tests on the eight NPD laminates, and $L = 75 \text{ mm}$ is the support span. The stress and strain were

calculated in the longitudinal x (1) and transverse y (2) and z (3) directions in the global (local) coordinate system. The 3D Tsai-Wu failure criterion factor was also computed based on the stresses in the local coordinate system to analyse the failure of the NPD laminate [34].

Fig. 2(a–c) shows the distribution of in-plane longitudinal normal stresses σ_x (σ_1), in-plane transverse normal stresses σ_y (σ_2), and interlaminar shear stresses τ_{xz} and τ_{yz} (τ_{13} and τ_{23}) in the global (local) coordinate system. The stresses σ_x , σ_1 , σ_y and σ_2 are linear within the plies but discontinuous between the plies; these normal stresses are antisymmetric about the neutral plane. The global shear stresses τ_{xz} and τ_{yz} are continuous through the thickness of the laminate. The global and local interlaminar shear stresses τ_{xz} , τ_{yz} , τ_{13} and τ_{23} are all symmetric about the neutral plane. The distribution of Tsai-Wu failure factor in the laminate is illustrated in Fig. 2(d).

4 Results

4.1 Static flexural behaviour

Fig. 3 shows the representative flexural stress–strain curves of the seven types of $[+45/-45/0]_{2s}$ CFRP laminates with or without pre-delamination. The flexural stress and strain were the effective values quantified using the measured bending load P and the midspan deflection D according to ASTM D790. As the deflections of all specimens were $>10\%$ of the support span, the effective flexural stress $\bar{\sigma}$ at the midpoint of the outer surface was approximated with a correction factor:

$$\bar{\sigma} = \left(\frac{3PL}{2bd^2} \right) \left(1 + 6 \left(\frac{D}{L} \right)^2 - 4 \frac{d}{L} \frac{D}{L} \right) \quad (2)$$

where $b = 12$ mm and $d = 2.13$ mm are the width and the thickness (depth) of the laminate specimen, respectively. The corresponding flexural strain ε was calculated as follows.

$$\varepsilon = \frac{6dD}{L^2} \quad (3)$$

The flexural stress–strain curve consists of the initial linear elastic deformation, subsequent nonlinear response, and final failure where the stress drops abruptly. The initial effective flexural modulus \overline{E}_0 was measured as the slope of the curve within the initial small deflection (<1% of the support span) where the correction factor can be ignored; thus the \overline{E}_0 can be calculated:

$$\overline{E}_0 = \frac{P_0 L^3}{4bd^3 D_0} \quad (4)$$

where P_0 is the initial load and D_0 is the initial deflection. The flexural stress–strain curve during reloading was also calculated for the seven types of laminates; only the curve for the PD1 specimen is shown in Fig. 3. Fig. 4 illustrates the effective flexural modulus at the initial elastic stage and the flexural strength at failure in the first loading and reloading. A deviation of <10% was achieved in the measured flexural properties, indicating the consistent material and experiment conditions.

4.2 Flexural failure modes

Fig. 5 shows the surface in the through-thickness edge of the laminate with no pre-delamination (NPD) after the flexural reloading failure. The optical microscopic examination reveals that the failure only appears in the 1st ply group, i.e., the compression zone of the laminate subjected to three-point bending (Fig. 5(a)). The SEM characterisation further exhibits the details of the failure modes in the plies

(Fig. 5(b–e)). Specifically, the fibre failure, matrix cracking and fibre/matrix debonding occur in the plies of the 1st group (Fig. 5(c–e)), and the delamination forms at the first (+45/–45), second (–45/0) and third (0/+45) interfaces near the top of the specimen (Fig. 5(b)). Note that both matrix cracking and fibre/matrix debonding cannot be differentiated in the low magnification SEM image, and thus they are identified as the transverse crack (Fig. 5(b)).

The fibre failure (i.e., micro-buckling or kinking) can be observed in the 0 ply of the 1st ply group (Fig. 5(c)). The length of fractured fibres (λ) is approximately equal to seven fibre diameters, which was also found in other laminates [27, 35]. The kinking band inclines with an angle (β) to the fibre direction. Exposed fibres are associated with ridges and valleys in the matrix in the two faces of the crack opening within the +45, –45 and 0 plies, implying the occurrence of fibre/matrix debonding [36] (Fig. 5(c–e)). The shear cusps as observed in Fig. 5(d, e) are the characteristics of matrix cracks arising due to the extensive localised yielding of the matrix.

Fig. 6 reveals the typical features of the delamination surfaces at the first (+45/–45), second (–45/0) and third (0/+45) interfaces in the 1st ply group. A majority of exposed fibres and the corresponding matrix valleys can be observed on the two faces of each delamination interface. This is the characteristic of the peel and shear fracture in fibre/matrix debonding [36]. The shear cusps oriented perpendicular to the matrix valleys also form between two adjacent valleys on the fracture surface; this is the result of the extensive localised yielding of the matrix caused by the shear stress in the interlaminar interfaces [37]. However, the quantity of exposed fibres (and matrix valleys) seems more than the shear cusps. This suggests that the delamination crack initiates and propagates along the fibre/matrix interface rather than within the matrix, probably because the fibre/matrix interface is weaker than the interlaminar epoxy in

the present study. Therefore, the dominant mechanism for delamination failure in the $[+45/-45/0]_{2s}$ laminate is fibre/matrix debonding instead of matrix cracking.

The SEM examination on the fracture surfaces of the laminates with the pre-delamination also reveal that similar to the NPD laminate, the failure modes including delamination, fibre failure, matrix cracking and fibre/matrix debonding mostly occur in the 1st ply group. All these failure modes as observed can be considered as the damage in the laminate subjected to flexural loads.

4.3 Internal 3D damage

X-ray microtomography on the laminates after the first flexural loading and failure characterises the details of the internal 3D damage within the plies that cannot be observed by optical microscopy. Figs. 7 and 8 show the typical damage in the laminates with no pre-delamination (NPD) and with pre-delamination (PD1, PD2, PD3, PD9, PD10 and PD11), respectively. Matrix cracking and fibre/matrix debonding cannot be distinguished in the μ XT images due to the limited resolution and the small fibre diameter; they are identified as the transverse cracking in Figs. 7 and 8. In the μ XT images, the surrounding composite materials (fibres and matrix) were hidden to better visualise the damage morphology and distribution. A good repeatability was achieved in the μ XT observations on the three specimens of each laminate type. To distinguish the different failure modes and the distribution (location), the delamination (blue), transverse crack (yellow), fibre failure (red) and embedded pre-delamination (black) were visualised with different colours. Moreover, the light, medium and dark colours further represent the damage in different plies and interfaces, as detailed in the legends of Figs. 7 and 8.

The μ XT of the NPD laminate reveals the 3D morphology of the delamination within the first (+45/-45), second (-45/0) and third (0/+45) interfaces in the 1st ply group (Fig. 7(a)). The full features of the transverse cracks and fibre failure can be observed in Fig. 7(b). The biggest damage of fibre failure occurs in the 0 ply and it continuously extends through the width of the specimen and perpendicular to the fibre directions. Most of the transverse crack planes in the +45 and -45 plies are parallel to the flexural loading direction. Note that this loading direction (i.e., the moving direction of the crosshead as shown in Fig. 5(a)) is perpendicular to the laminate plane. But the transverse crack planes in the 0 ply are perpendicular to the loading direction. The delamination is interconnected with the transverse cracks and fibre failure in the adjacent plies; moreover, the transverse cracks join the fibre failure in the same ply.

Similar to the NPD laminate, the in-ply and interlaminar failure modes and the 3D patterns (location or distribution) can be found in the other six types of laminates with pre-delamination (PD1, PD2, PD3, PD9, PD10 and PD11) as shown in Fig. 8. However, some differences and exceptions exist in these laminates due to the effect of pre-delamination at various interfaces. These phenomena are highlighted as follows.

- In the PD1 laminate (Fig. 8(a)), the fibre failure interconnects the two transverse cracks within the +45 ply; and the fibres in the 0 ply fail along the transverse crack propagation direction in the adjacent -45 ply. It seems that the transverse crack can provoke the fibre failure as the transverse strength is less than the longitudinal strength of the UD laminae (Table 2).
- In the PD2 laminate (Fig. 8(b)), no delamination forms in the +45/-45 interface with no transverse cracks in the +45 ply and no fibre failure in the +45 or -45 plies. The transverse cracks in the -45 ply is the only damage above the -45/0 interface where the pre-delamination is embedded.

- In the PD3 laminate (Fig. 8(c)), the fibres in the +45 and –45 plies do not fail.
- In the PD9 and PD10 laminates (Figs. 8(d, e)), the damage size (e.g. delamination) in the 1st group is different from that in the NPD laminate, despite the similarity in their damage patterns. No new delamination forms at the interface for the embedded pre-delamination.
- In the PD11 laminate (Fig. 8(f)), new delamination develops from the embedded pre-delamination at the –45/+45 interface with the transverse cracks in the adjacent +45 ply.

5 Discussion

5.1 Correlation between stress and failure

In the [+45/–45/0]_{2s} laminate with no pre-delamination, only the normal stresses σ_1 (compressive) and σ_2 (tensile) in the 0 ply of the 1st group exceed the longitudinal compressive strength X_c and the transverse tensile strength Y_t , respectively (refer to Fig. 2(a, b) and Table 2). The highest Tsai-Wu failure factor (>1.0) also exists in the same ply (Fig. 2(d)). Therefore, the fibre failure and transverse cracking (matrix cracking and fibre/matrix debonding) occur in the 0 ply of the 1st group as shown in Fig. 5. After the failure in this 0 ply, the stresses re-distribute and they can concentrate in the adjacent plies, e.g., both the +45 and –45 plies in the 1st and 2nd groups. The normal stresses (σ_1 and σ_2) and Tsai-Wu factor in the +45 and –45 plies of the 1st group are relatively greater than those in the 2nd group (Fig. 2(a, b, d)). Thus this new stress concentration results in the failure in the neighbouring +45 and –45 plies of the 1st group in the NPD laminate (Fig. 5).

The overall stress distribution in the laminates with pre-delamination (PD1, PD2, PD3, PD9, PD10 and PD11) is expected to be similar to that in the NPD laminate.

This is because the pre-delamination (144 mm^2) affects the localised stress distribution adjacent to it but has little impact on the overall distribution. Both the SEM and μXT observations show similar in-ply and interlaminar failure modes in the laminates with or without pre-delamination. The delamination, transverse cracks (matrix cracks and fibre/matrix debonding) and fibre failure dominantly occur through the thickness in the 1st ply group of the $[+45/-45/0]_{2s}$ CFRP laminates after flexural failure. The failure modes within the plies include the fibre failure, matrix cracking and fibre/matrix debonding. Delamination is the failure mode between the plies, for which fibre/matrix debonding is the primary mechanism while matrix cracking the secondary mechanism. The in-ply and interlaminar failure modes in these multidirectional laminates may interact with one another; such interaction need to be considered for the reliable prediction of service performance.

5.2 *Effect of pre-delamination on flexural behaviour*

Despite the similarity in damage distribution, the location and size of the damage can be affected by the embedded pre-delamination at the interface. The location of some damage in the PD2, PD3 and PD11 laminates is different from that in the NPD laminate. The Tsai-Wu factor in the +45 and -45 plies of the 4th group exceeds 1.0 in the NPD laminate (Fig. 2(d)), but the two plies do not fail probably because much energy is released during the failure in the 1st group. However in the PD11 laminate, the embedded pre-delamination may lead to the increased Tsai-Wu failure factor in the outer +45 ply in the 4th group, and the new delamination developed at the -45/+45 interface with the transverse cracks in the adjacent +45 ply. Even though the damage locations in the PD1, PD9 and PD10 laminates seem similar to the NPD laminate, the embedded pre-delamination affects the damage size.

The areas of delamination (excluding pre-delamination), transverse cracks and fibre failure in the 1st ply group in the seven types of laminates were calculated from the μ XT images using the AVIZO/FIRE software. The damage area was chosen instead of the damage volume as in some literature [24], because the opening displacement of the delamination damage is arbitrary and random. Fig. 9(a) demonstrates the delamination areas at the three interfaces in the 1st ply group of the seven types of laminates. The embedded pre-delamination was excluded from the delamination damage in the calculation. The largest delamination is located at the third (0/+45) interface among the three interfaces probably due to the high strain energy release rate for delamination at this interface [23]. The smallest delamination is at the first (+45/-45) interface for all the laminates except PD1 (Fig. 9(a)); in particular the delamination area at the first interface is zero in the PD2 laminate (Fig. 8(b)). For the PD1 laminate, the delamination area at the first (+45/-45) is slightly larger than that at the second (-45/0) interface because the pre-delamination at the first interface leads to more delamination damage at the same interface under flexural loads.

The embedded pre-delamination has little influence on the initial flexural modulus but has a significant impact on the flexural strength at failure in the laminates (Fig. 4). The modulus of the seven laminates at initial loading is almost the same because the interlaminar plane of pre-delamination damage is perpendicular to the bending load direction. The pre-delamination reduces the flexural strength and strain at failure (Figs. 3 and 4). But the extent of such negative effects on the strength can be different, depending on the location of the embedded pre-delamination. Specifically, the flexural strength of the [+45/-45/0]_{2s} laminate is more sensitive to

the pre-delamination embedded at the third interface (0/+45), but less sensitive to that at the ninth interface (+45/0).

5.3 *Effect of damage on flexural properties after reloading*

All the damage observed in the seven types of laminates can be grouped into two types according to the orientation of the damage plane relative to the flexural loading direction (crosshead motion direction). First, the perpendicular damage includes the delamination in all the interfaces and the transverse cracks in the 0 ply; the plane of the damage is perpendicular to the flexural loading direction. Second, the transverse cracks in the 45 and -45 plies and the fibre failure in all the plies are categorised as the parallel damage, since the damage plane is parallel to the loading direction. The calculated areas of the perpendicular damage are plotted in Fig. 9(b), whilst the parallel damage area are in Fig. 9(c). The damage area is compared to the reduction of flexural properties after flexural reloading. The reduction ratios of flexural strength and modulus (Fig. 9(b, c)) were calculated based on the measured properties at the first loading and the residual properties at reloading (Fig. 4). The areas of perpendicular (parallel) damage formed at loading are almost positively correlated with the reduction of flexural strength (modulus) by subsequent reloading.

6 **Conclusions**

Static three-point bending flexural experiments were performed on the [+45/-45/0]_{2s} CFRP laminates with or without the pre-delamination embedded at different interfaces. After flexural failure, the internal 3D damage was characterised and quantified in the X-ray microtomography; and the failure modes were examined in the SEM. The following conclusions were drawn.

- The in-ply and interlaminar failure modes were similar among all the laminates with or without the pre-delamination. The fibre failure, matrix cracking and fibre/matrix debonding occur within the plies of the 1st group and the delamination forms at the three interfaces of this group. The stress analysis by the classical laminate theory reveals that the laminate with no pre-delamination starts to fail in the 0 ply of the 1st group, which agrees with the SEM and μ XT observations of fibre failure and transverse cracking (matrix cracking and fibre/matrix debonding) in the ply.
- However, the pre-delamination embedded at different interfaces influences the location and size of the damage (various failure modes) and thus the flexural properties. The pre-delamination effect on flexural properties can be different, depending on the location of the embedded pre-delamination. The pre-delamination reduces the flexural strength and strain at failure. The flexural strength is the most sensitive to the pre-delamination embedded at the third interface but the least sensitive to that at the ninth interface.
- The new formed damage by flexural loading can affect the residual properties of the laminate after subsequent reloading. The area of perpendicular (parallel) damage is almost positively correlated with the reduction of flexural strength (modulus) by reloading.

Acknowledgements

This work was financially supported by the Ministry of Defence Singapore – Nanyang Technological University (NTU) Joint Applied R&D Cooperation (JPP) Programme (Grant No.: MINDEF-NTU-JPP/12/01/02). ZL acknowledges the NTU Interdisciplinary Graduate School Research Student Scholarship.

References

- [1] Meng M, Rizvi MJ, Grove SM, Le HR. Effects of hygrothermal stress on the failure of CFRP composites. *Compos Struct* 2015;133:1024-1035.
- [2] Veers PS, Ashwill TD, Sutherland HJ, Laird DL, Lobitz DW, Griffin DA, et al. Trends in the design, manufacture and evaluation of wind turbine blades. *Wind Energy* 2003;6(3):245-259.
- [3] Aslan Z, Sahin M. Buckling behavior and compressive failure of composite laminates containing multiple large delaminations. *Compos Struct* 2009;89(3):382-390.
- [4] Brunner AJ, Murphy N, Pinter G. Development of a standardized procedure for the characterization of interlaminar delamination propagation in advanced composites under fatigue mode I loading conditions. *Eng Fract Mech* 2009;76(18):2678-2689.
- [5] Kensch CW. Fatigue of composites for wind turbines. *Int J Fatigue* 2006;28(10):1363-1374.
- [6] Sakin R, Ay I, Yaman R. An investigation of bending fatigue behavior for glass-fiber reinforced polyester composite materials. *Mater Des* 2008;29(1):212-217.
- [7] Liu Z, Li P, Srikanth N, Liu T, Chai GB. Quantification of flexural fatigue life and 3D damage in carbon fibre reinforced polymer laminates. *Compos Part A* 2016;90:778-785.
- [8] Mathew J, Ramakrishnan N, Naik NK. Trepanning on unidirectional composites: delamination studies. *Compos Part A* 1999;30(8):951-959.
- [9] Valdes SHD, Soutis C. Delamination detection in composite laminates from variations of their modal characteristics. *J Sound Vibr* 1999;228(1):1-9.
- [10] Keilers CH, Chang FK. IDENTIFYING DELAMINATION IN COMPOSITE BEAMS USING BUILT-IN PIEZOELECTRICS .1. EXPERIMENTS AND ANALYSIS. *J Intell Mater Syst Struct* 1995;6(5):649-663.
- [11] Cappello F, Tumino D. Numerical analysis of composite plates with multiple delaminations subjected to uniaxial buckling load. *Compos Sci Technol* 2006;66(2):264-272.
- [12] Pascoe JA, Rans CD, Benedictus R. Characterizing fatigue delamination growth behaviour using specimens with multiple delaminations: The effect of unequal delamination lengths. *Eng Fract Mech* 2013;109:150-160.

- [13] Wang XW, Pont-Lezica I, Harris JM, Guild FJ, Pavier MJ. Compressive failure of composite laminates containing multiple delaminations. *Compos Sci Technol* 2005;65(2):191-200.
- [14] Lemanski SL, Wang J, Sutcliffe MPF, Potter KD, Wisnom MR. Modelling failure of composite specimens with defects under compression loading. *Compos Part A* 2013;48:26-36.
- [15] Chen HR, Sun XN. Residual compressive strength of laminated plates with delamination. *Compos Struct* 1999;47(1-4):711-717.
- [16] Huang R, Li P, Liu T. X-ray microtomography and finite element modelling of compressive failure mechanism in cenosphere epoxy syntactic foams. *Compos Struct* 2016;140:157-165.
- [17] Huang R, Li P, Wang Z, Liu T. X-ray microtomographic characterization and quantification of the strain rate dependent failure mechanism in cenosphere epoxy syntactic foams. *Adv Eng Mater* 2016;18(9):1550-1555.
- [18] Liu T, Huang R, Li P. Cone-beam CT reconstruction along any orientation of interest. *J X-Ray Sci Technol* 2015;23(6):773-782.
- [19] Tan KT, Watanabe N, Iwahori Y. X-ray radiography and micro-computed tomography examination of damage characteristics in stitched composites subjected to impact loading. *Compos Part B* 2011;42(4):874-884.
- [20] Aroush DRB, Maire E, Gauthier C, Youssef S, Cloetens P, Wagner HD. A study of fracture of unidirectional composites using in situ high-resolution synchrotron X-ray microtomography. *Compos Sci Technol* 2006;66(10):1348-1353.
- [21] Bull DJ, Spearing SM, Sinclair I, Helfen L. Three-dimensional assessment of low velocity impact damage in particle toughened composite laminates using micro-focus X-ray computed tomography and synchrotron radiation laminography. *Compos Part A* 2013;52:62-69.
- [22] Dunkers JP, Sanders DP, Hunston DL, Everett MJ, Green WH. Comparison of optical coherence tomography, x-ray computed tomography, and confocal microscopy results from an impact damaged epoxy/E-glass composite. *J Adhes* 2002;78(2):129-154.
- [23] Lambert J, Chambers AR, Sinclair I, Spearing SM. 3D damage characterisation and the role of voids in the fatigue of wind turbine blade materials. *Compos Sci Technol* 2012;72(2):337-343.

- [24] McCombe GP, Rouse J, Trask RS, Withers PJ, Bond IP. X-ray damage characterisation in self-healing fibre reinforced polymers. *Compos Part A* 2012;43(4):613-620.
- [25] Moffat AJ, Wright P, Buffiere JY, Sinclair I, Spearing SM. Micromechanisms of damage in 0 degrees splits in a 90/0 (s) composite material using synchrotron radiation computed tomography. *Scr Mater* 2008;59(10):1043-1046.
- [26] Schilling PJ, Karedla BPR, Tatiparthi AK, Verges MA, Herrington PD. X-ray computed microtomography of internal damage in fiber reinforced polymer matrix composites. *Compos Sci Technol* 2005;65(14):2071-2078.
- [27] Meng M, Le HR, Rizvi MJ, Grove SM. 3D FEA modelling of laminated composites in bending and their failure mechanisms. *Compos Struct* 2015;119:693-708.
- [28] Koricho EG, Belingardi G, Beyene AT. Bending fatigue behavior of twill fabric E-glass/epoxy composite. *Compos Struct* 2014;111:169-178.
- [29] Tserpes KI, Papanikos P, Labeas G, Pantelakis S. Fatigue damage accumulation and residual strength assessment of CFRP laminates. *Compos Struct* 2004;63(2):219-230.
- [30] Liu T. Cone-beam CT reconstruction for planar object. *NDT&E Int* 2012;45(1):9-15.
- [31] Creemers RJC. Interlaminar shear strength criteria for composites. 2010.
- [32] Lu G, Liu Y, Zhang C. Three-dimensional finite element progressive failure analysis of composite laminates containing a hole under axial extension. *Journal of Nanjing University of Aeronautics & Astronautics* 2009;2009-01.
- [33] Kollár LP, Springer GS. *Mechanics of Composite Structures*: Cambridge University Press; 2003.
- [34] Tsai SW, Wu EM. A General Theory of Strength for Anisotropic Materials. *J Compos Mater* 1971;5(1):58-80.
- [35] Soutis C. Measurement of the static compressive strength of carbon-fibre/epoxy laminates. *Compos Sci Technol* 1991;42(4):373-392.
- [36] Hibbs MF, Bradley WL. Correlations between micromechanical failure processes and the delamination toughness of graphite/epoxy systems. *Fractography of Modern Engineering Materials: Composites and Metals: ASTM STP948*; 1987. p. 68-97.

[37] Morris GE. Determining Fracture Directions and Fracture Origins on Failed Graphite/Epoxy Surfaces. In: Pipes RB, editor. *Nondestructive Evaluation and Flaw Criticality for Composite Materials*: ASTM STP696; 1979. p. 174-297.

List of Tables

Table 1 The ply configuration of carbon fibre reinforced polymer (CFRP) laminates with the pre-delamination at different interfaces (PD1, PD2, PD3, PD9, PD10 and PD11) or no pre-delamination (NPD).

Laminate type	Ply configuration
NPD	[+45/-45/0/+45/-45/0/0/-45/+45/0/-45/+45]
PD1	[+45/PD/-45/0/+45/-45/0/0/-45/+45/0/-45/+45]
PD2	[+45/-45/PD/0/+45/-45/0/0/-45/+45/0/-45/+45]
PD3	[+45/-45/0/PD/+45/-45/0/0/-45/+45/0/-45/+45]
PD9	[+45/-45/0/+45/-45/0/0/-45/+45/PD/0/-45/+45]
PD10	[+45/-45/0/+45/-45/0/0/-45/+45/0/PD/-45/+45]
PD11	[+45/-45/0/+45/-45/0/0/-45/+45/0/-45/PD/+45]

Table 2 Measured anisotropic mechanical properties of unidirectional laminae.

Parameter *	Value
Longitudinal Young's modulus (GPa), E_1	134
Transverse Young's modulus (GPa), $E_2=E_3$	6.56
Poisson ratio in 1-2 and 1-3 planes, $\nu_{12}=\nu_{13}$	0.232
Poisson ratio in 2-3 planes, ν_{23}	0.3
Shear modulus in 1-2 and 1-3 planes (GPa), $G_{12}=G_{13}$	5.60
Shear modulus in 2-3 planes (GPa), G_{23}	2.52
In-plane longitudinal tensile strength (MPa), X_t	2173
In-plane longitudinal compressive strength (MPa), X_c	952
In-plane transverse tensile strength (MPa), Y_t	30
In-plane transverse compressive strength (MPa), Y_c	124
Out-of-plane tensile strength (MPa), Z_t	30
Out-of-plane compressive strength (MPa), Z_c	124
Shear strength in 1-2 and 1-3 planes (MPa), $S_{12}=S_{13}$	110
Shear strength in 2-3 plane (MPa), S_{23}	110

* The subscripts 1, 2 and 3 represent the directions in the local coordinate of unidirectional laminae: 1 is the fibre direction, 2 is transverse to the fibre but in the plane of a fibre ply, and 3 is the direction perpendicular to the ply. The subscripts t and c represent tension and compression, respectively.

List of Figures

Fig. 1 The schematic of the carbon fibre reinforced polymer (CFRP) laminate with an embedded Teflon layer as the pre-delamination, and the rectangular specimens machined from the laminate by waterjet cutting.

Fig. 2 The predictions of (a) in-plane longitudinal normal stresses, (b) in-plane transverse normal stresses, (c) interlaminar shear stresses, and (d) Tsai-Wu failure factor in the CFRP laminate with no pre-delamination (NPD) subjected to static three-point bending at the failure load 343 N using classical laminate theory.

Fig. 3 The representative flexural stress–strain curves of CFRP laminates with or without the pre-delamination subjected to static three-point bending and subsequent reloading. Note that the reloading curve is shown for the PD1 specimen only.

Fig. 4 (a) Flexural modulus and (b) flexural strength of CFRP laminates as a function of pre-delamination location.

Fig. 5 The CFRP laminate with no pre-delamination (NPD) after static three-point bending testing: (a) optical image of the through-thickness edge; (b–e) SEM images of the edge surface in the 1st ply group near the failure site. The overview of the failure in the 1st ply group is shown in (b) while the details in each ply are in (c–e).

Fig. 6 SEM images of the delamination surfaces in the ply interfaces in the 1st groups in the CFRP laminate with no pre-delamination (NPD).

Fig. 7 X-ray microtomographic observations of the damage in the CFRP laminate with no pre-delamination (NPD) subjected to static three-point bending. The delamination in the 1st ply group is denoted in (a) while the transverse cracks and fibre failure are in (b). The delamination at the –45/0 interface is hidden in (b) to better illustrate the damage.

Fig. 8 X-ray microtomographic observations of the damage in the CFRP laminate with the pre-delamination at different interfaces subjected to static three-point bending. The 3D overview of the damage in the laminate is illustrated in the left figure, while the damage in the 1st ply group is detailed in the right figure in which the pre-delamination is hidden.

Fig. 9 (a) Projected delamination areas at the three interfaces in the 1st ply group in the CFRP laminates as a function of pre-delamination location. (b) Comparison between the areas of the damage perpendicular to the loading direction and the reduction of flexural strength by reloading. (c) Comparison between the areas of the damage parallel to the loading direction and the reduction of flexural modulus by reloading. The pre-delamination is excluded

from the calculation of the delamination damage. The error bars for the reduction of flexural properties are not shown in (b, c).

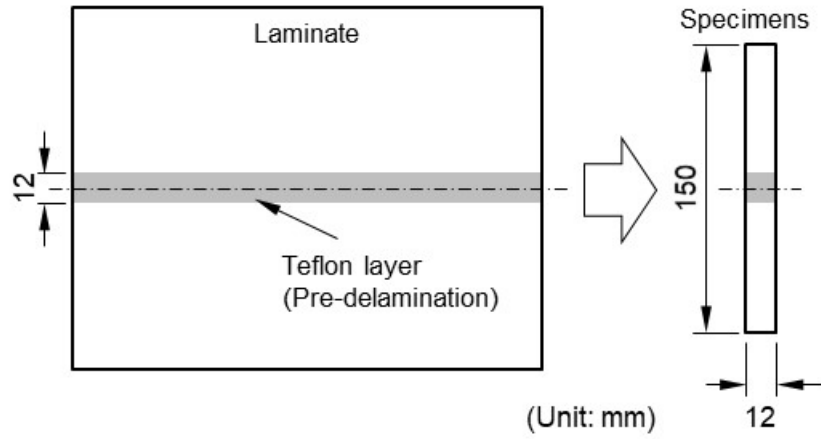


Figure 1: The schematic of the carbon fibre reinforced polymer (CFRP) laminate with an embedded Teflon layer as the pre-delamination, and the rectangular specimens machined from the laminate by waterjet cutting.

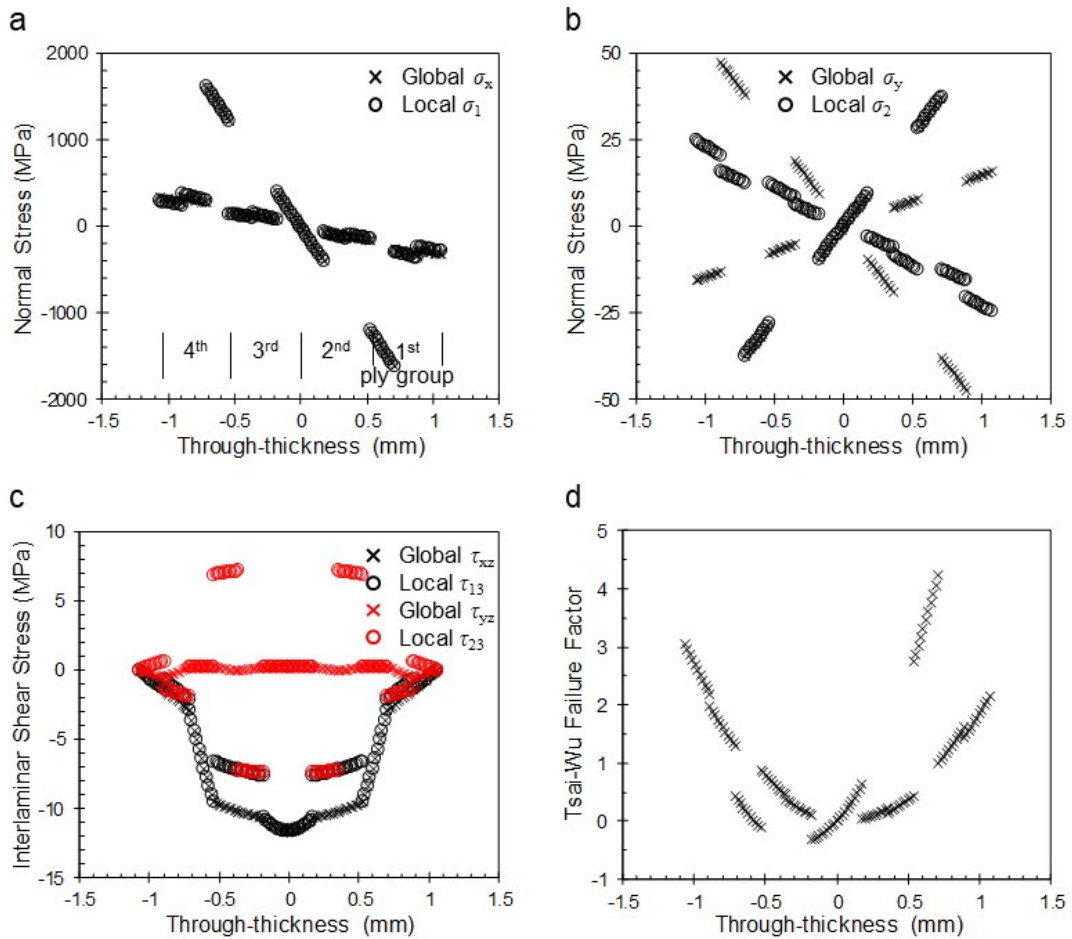


Figure 2: The predictions of (a) in-plane longitudinal normal stresses, (b) in-plane transverse normal stresses, (c) interlaminar shear stresses, and (d) Tsai-Wu failure factor in the CFRP laminate with no pre-delamination (NPD) subjected to static three-point bending at the failure load 343 N using classical laminate theory.

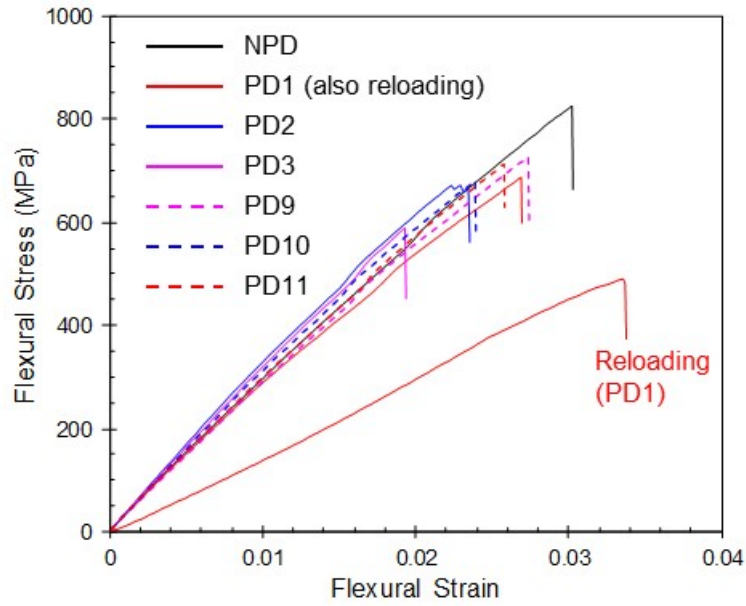


Figure 3: The representative flexural stress–strain curves of CFRP laminates with or without the pre-delamination subjected to static three-point bending and subsequent reloading. Note that the reloading curve is shown for the PD1 specimen only.

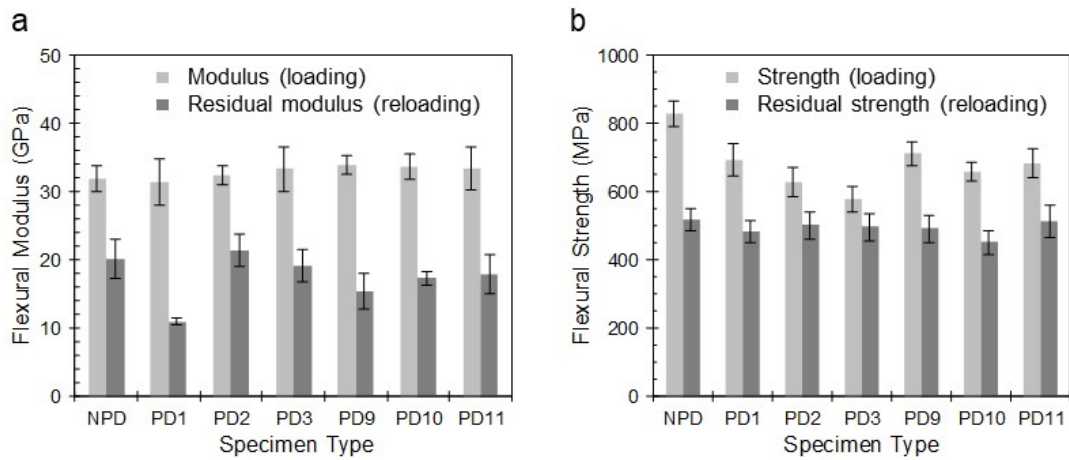


Figure 4: (a) Flexural modulus and (b) flexural strength of CFRP laminates as a function of pre-delamination location.

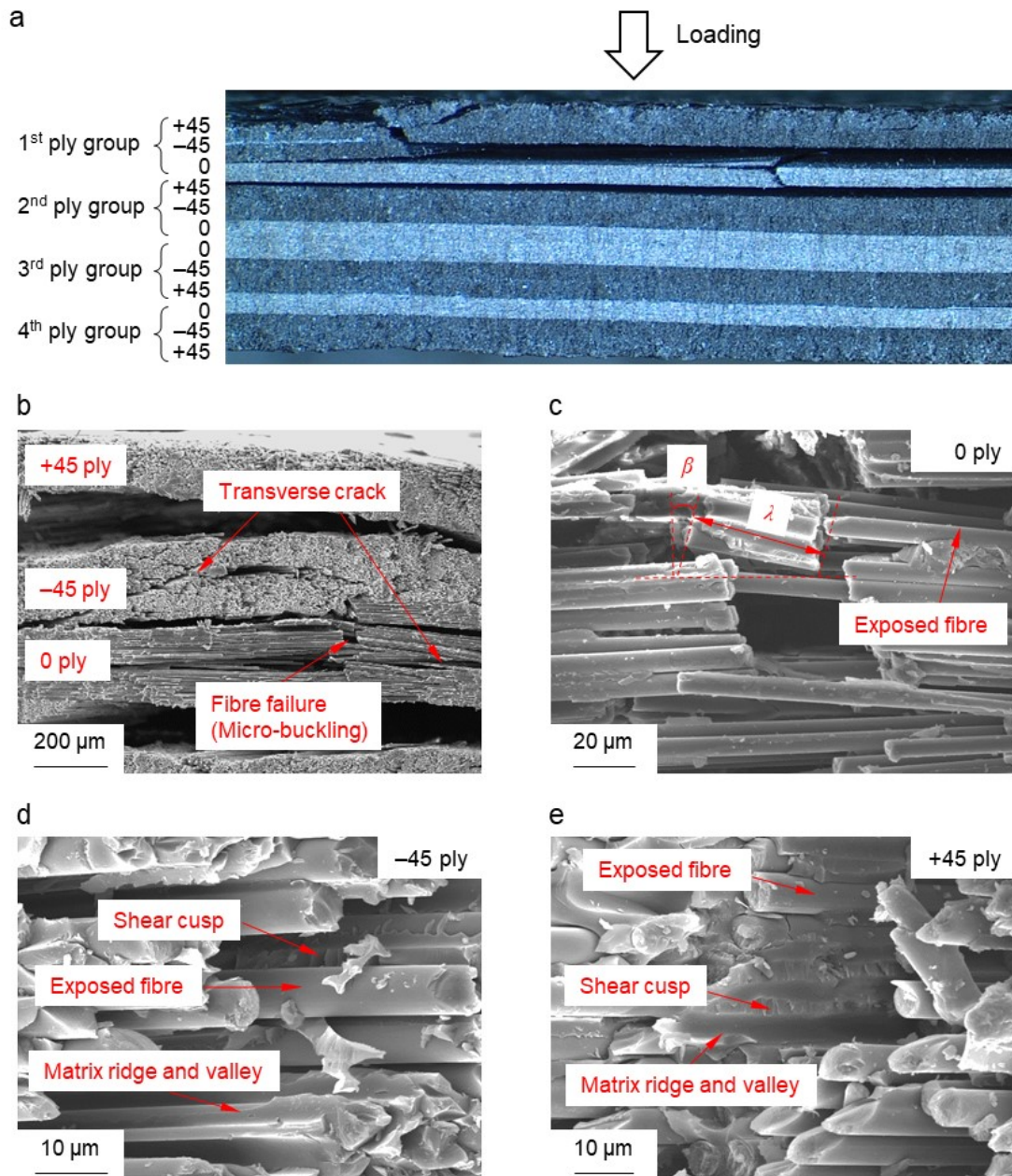


Figure 5: The CFRP laminate with no pre-delamination (NPD) after static three-point bending testing: (a) optical image of the through-thickness edge; (b–e) SEM images of the edge surface in the 1st ply group near the failure site. The overview of the failure in the 1st ply group is shown in (b) while the details in each ply are in (c–e).

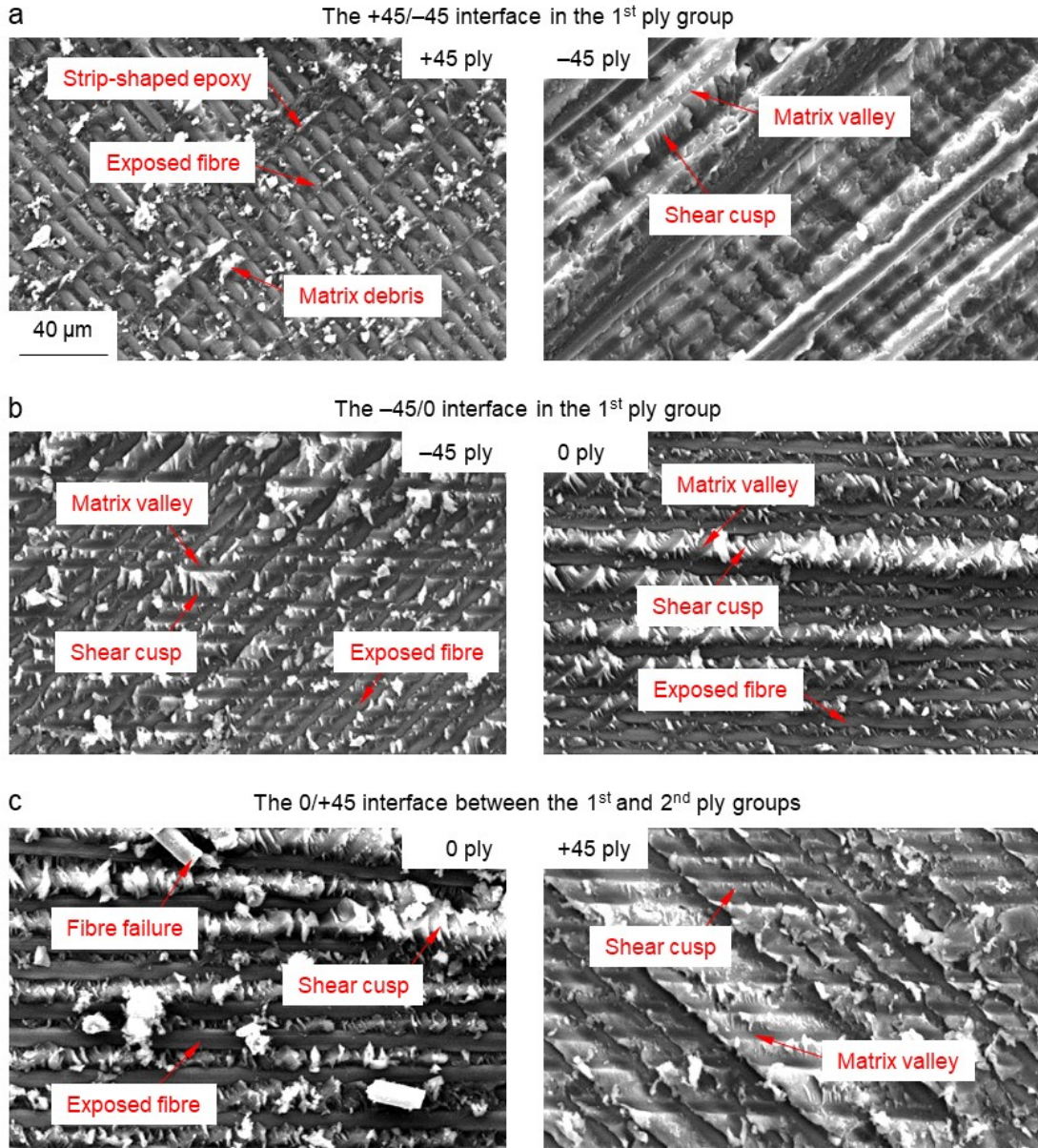


Figure 6: SEM images of the delamination surfaces in the ply interfaces in the 1st groups in the CFRP laminate with no pre-delamination (NPD).

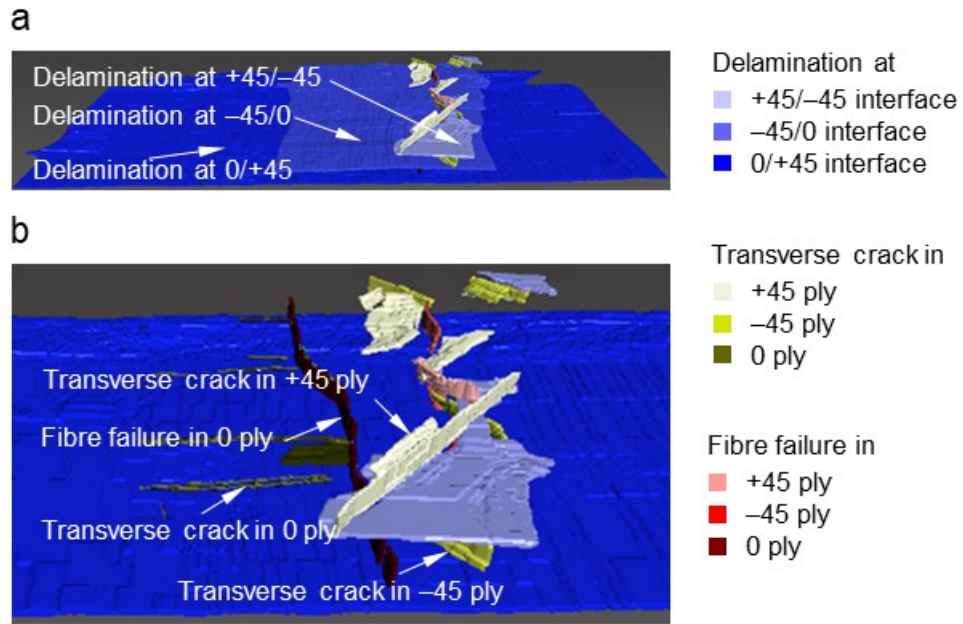


Figure 7: X-ray microtomographic observations of the damage in the CFRP laminate with no pre-delamination (NPD) subjected to static three-point bending. The delamination in the 1st ply group is denoted in (a) while the transverse cracks and fibre failure are in (b). The delamination at the -45/0 interface is hidden in (b) to better illustrate the damage.

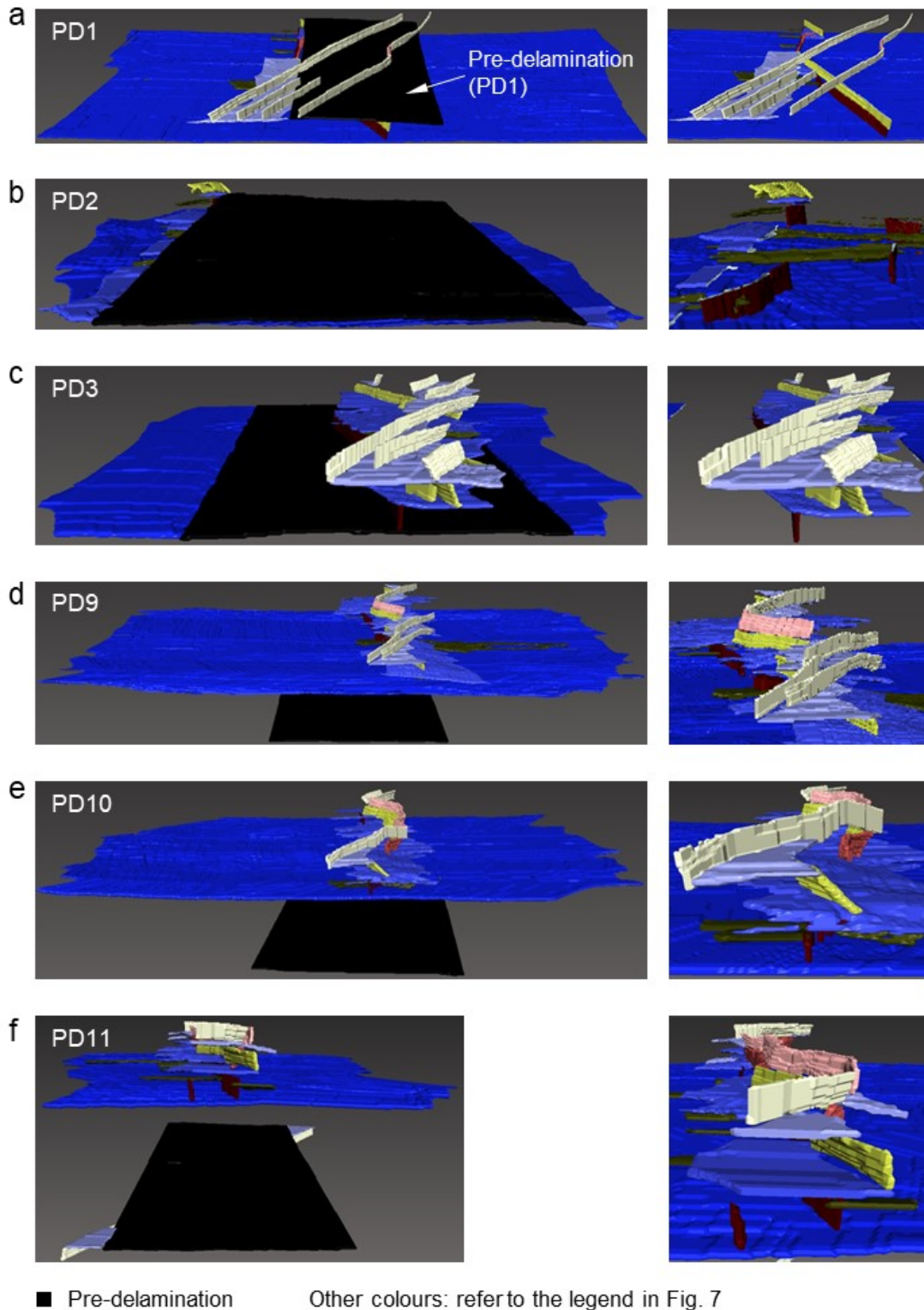


Figure 8: X-ray microtomographic observations of the damage in the CFRP laminate with the pre-delamination at different interfaces subjected to static three-point bending. The 3D overview of the damage in the laminate is illustrated in the left figure, while the damage in the 1st ply group is detailed in the right figure in which the pre-delamination is hidden.

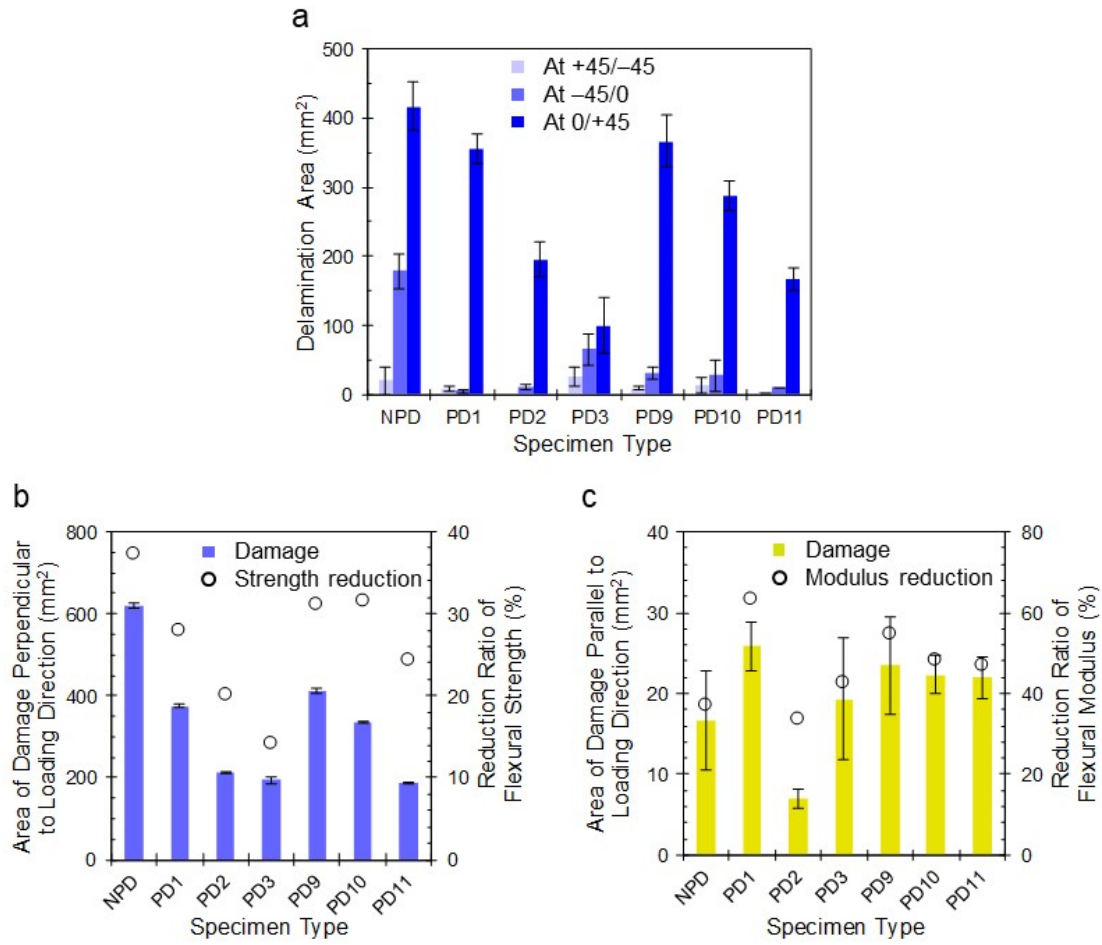


Figure 9: (a) Projected delamination areas at the three interfaces in the 1st ply group in the CFRP laminates as a function of pre-delamination location. (b) Comparison between the areas of the damage perpendicular to the loading direction and the reduction of flexural strength by reloading. (c) Comparison between the areas of the damage parallel to the loading direction and the reduction of flexural modulus by reloading. The pre-delamination is excluded from the calculation of the delamination damage. The error bars for the reduction of flexural properties are not shown in (b, c).